

## Supporting Information

for *Adv. Funct. Mater.*, DOI: 10.1002/adfm.202300089

Perovskite Solar Cells Consisting of PTAA Modified with Monomolecular Layer and Application to All-Perovskite Tandem Solar Cells with Efficiency over 25%

*Huan Bi, Yasuhiro Fujiwara, Gaurav Kapil, Daiva Tavgeniene, Zheng Zhang, Liang Wang, Chao Ding, Shahrir Razey Sahamir, Ajay Kumar Baranwal, Yoshitaka Sanehira, Kitamura Takeshi, Guozheng Shi, Takeru Bessho, Hiroshi Segawa,\* Saulius Grigalevicius,\* Qing Shen,\* and Shuzi Hayase\**

# Supporting Information

## **Perovskite Solar Cells Consisting of PTAA Passivated with Monomolecular Layer and Application to All-perovskite Tandem Solar Cells with Efficiency over 25%**

*Huan Bi<sup>1,2</sup>, Yasuhiro Fujiwara<sup>1</sup>, Gaurav Kapil<sup>1</sup>, Daiva Tavgeniene<sup>3</sup>, Zheng Zhang<sup>1,2</sup>, Liang Wang<sup>1</sup>, Chao Ding<sup>2</sup>, Shahrir Razey Sahamir<sup>1</sup>, Ajay Kumar Baranwal<sup>1</sup>, Yoshitaka Sanehira<sup>1</sup>, Kitamura Takeshi<sup>1</sup>, Guozheng Shi<sup>2</sup>, Takeru Bessho<sup>4</sup>, Hiroshi Segawa<sup>4\*</sup>, Saulius Grigalevicius<sup>3\*</sup>, Qing Shen<sup>1\*</sup>, and Shuzi Hayase<sup>1\*</sup>*

<sup>1</sup>i-Powered Energy System Research Center (i-PERC), The University of Electro-Communications, 1-5-1 Chofugaoka, Chofu, Tokyo, 182-8585, Japan.

<sup>2</sup>Faculty of Informatics and Engineering, The University of Electro-Communications, 1-5-1 Chofugaoka, Chofu, Tokyo, 182-8585, Japan.

<sup>3</sup>Department of Polymer Chemistry and Technology, Kaunas University of Technology, Radvilenu Plentas 19, LT50254 Kaunas, Lithuania.

<sup>4</sup>Research Center for Advanced Science and Technology, The University of Tokyo, 4-6-1 Komaba, Meguro-ku, Tokyo 153-8904, Japan.

### **Corresponding Authors:**

E-mail:

H. Segawa: csegawa@mail.ecc.u-tokyo.ac.jp;

S. Grigalevičius: saulius.grigalevicius@ktu.lt;

Q. Shen: shen@pc.uec.ac.jp;

S. Hayase: hayase@uec.ac.jp.

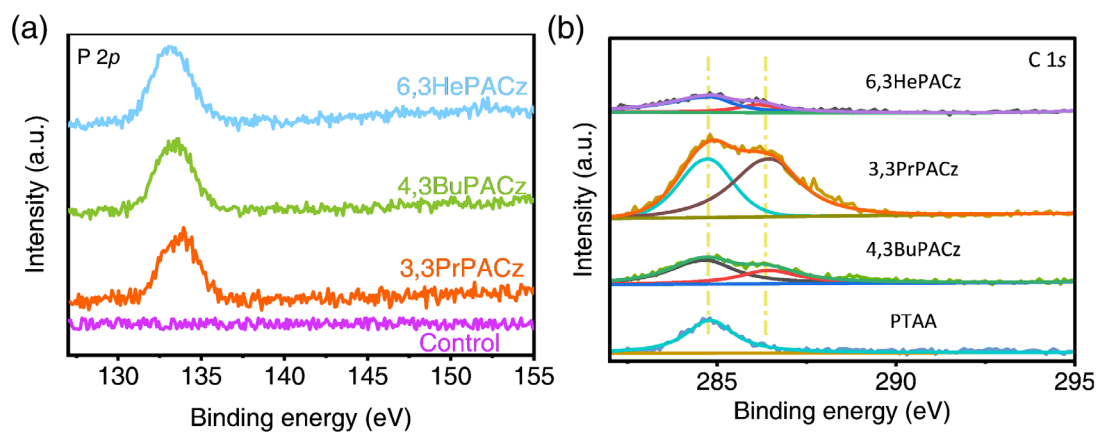


Figure S1. XPS of the (a) P 2p and (b) C 1s on the substance of PTAA, 3,3PrPACz/PTAA, 6,3HePACz/PTAA, and 4,3BuPACz/PTAA.

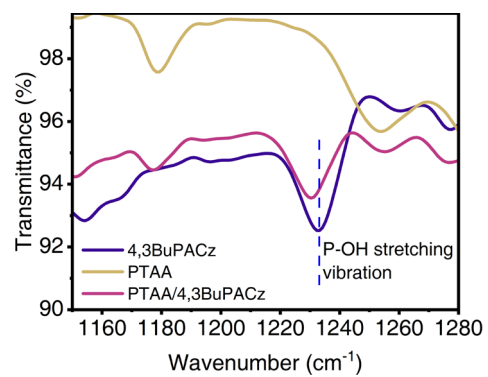


Figure S2. FTIR spectra of the PTAA films, 4,3BuPACz film and the PTAA/4,3BuPACz film.

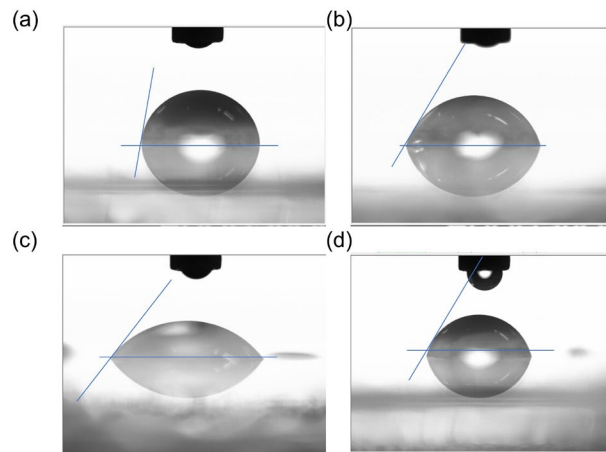


Figure S3. Images of the perovskite solution contact angle with the substrate of (a) PTAA, (b) PTAA/3,3PrPACz, (c) PTAA/4,3BuPACz and (d) PTAA/6,3HePACz.

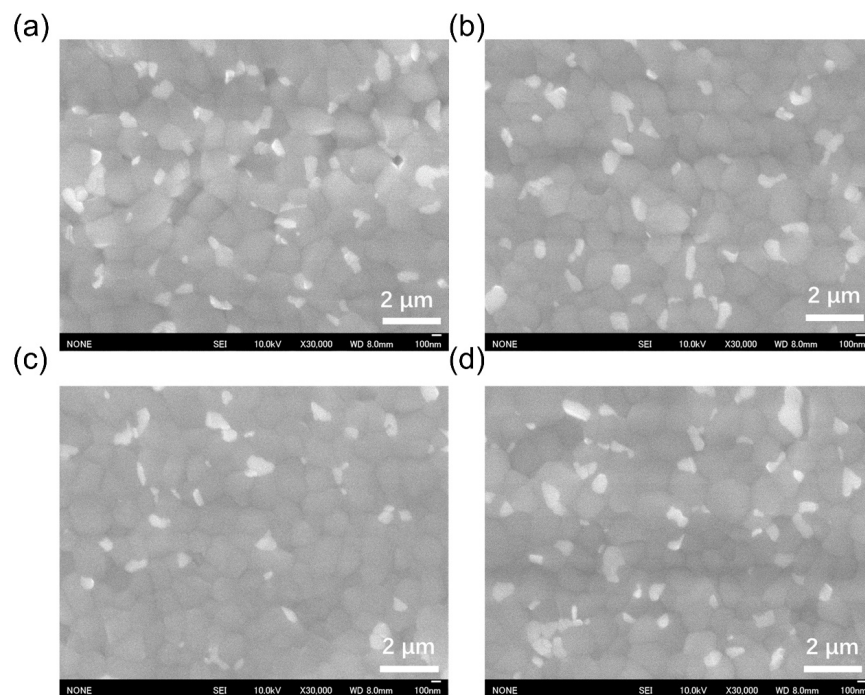


Figure S4. Top-view SEM images of the perovskite films prepared on PTAA modified by (a) None, (b) 3,3PrPACz, (c) 4,3BuPACz and (d) 6,3HePACz.

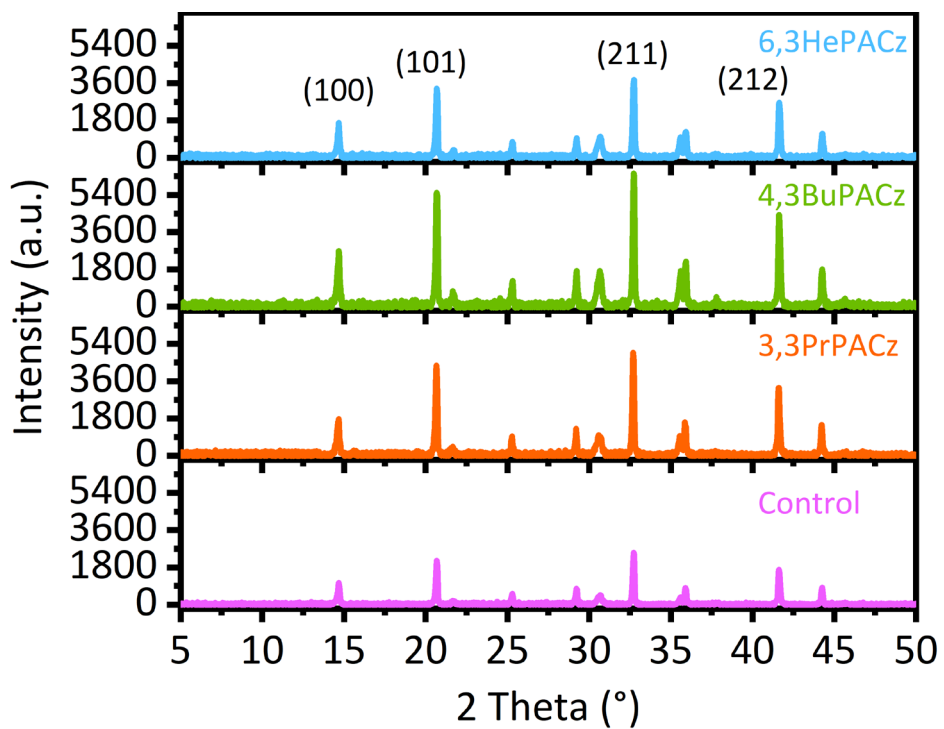


Figure S5. XRD patterns of the perovskite films based on PTAA with or without monolayer modification.

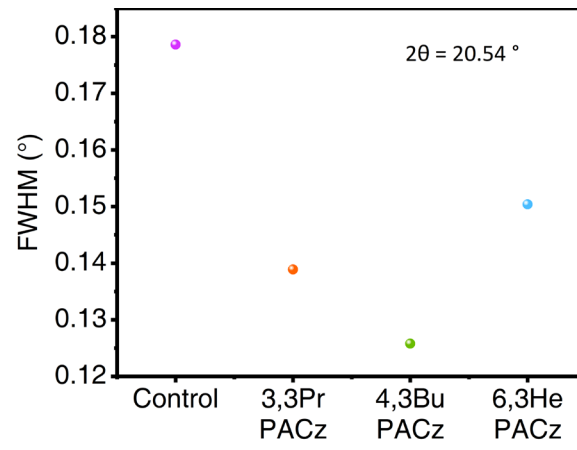


Figure S6. Summarized of the full width at half maximum (FWHM) of the perovskite ((101) plane) deposited on different substrate.

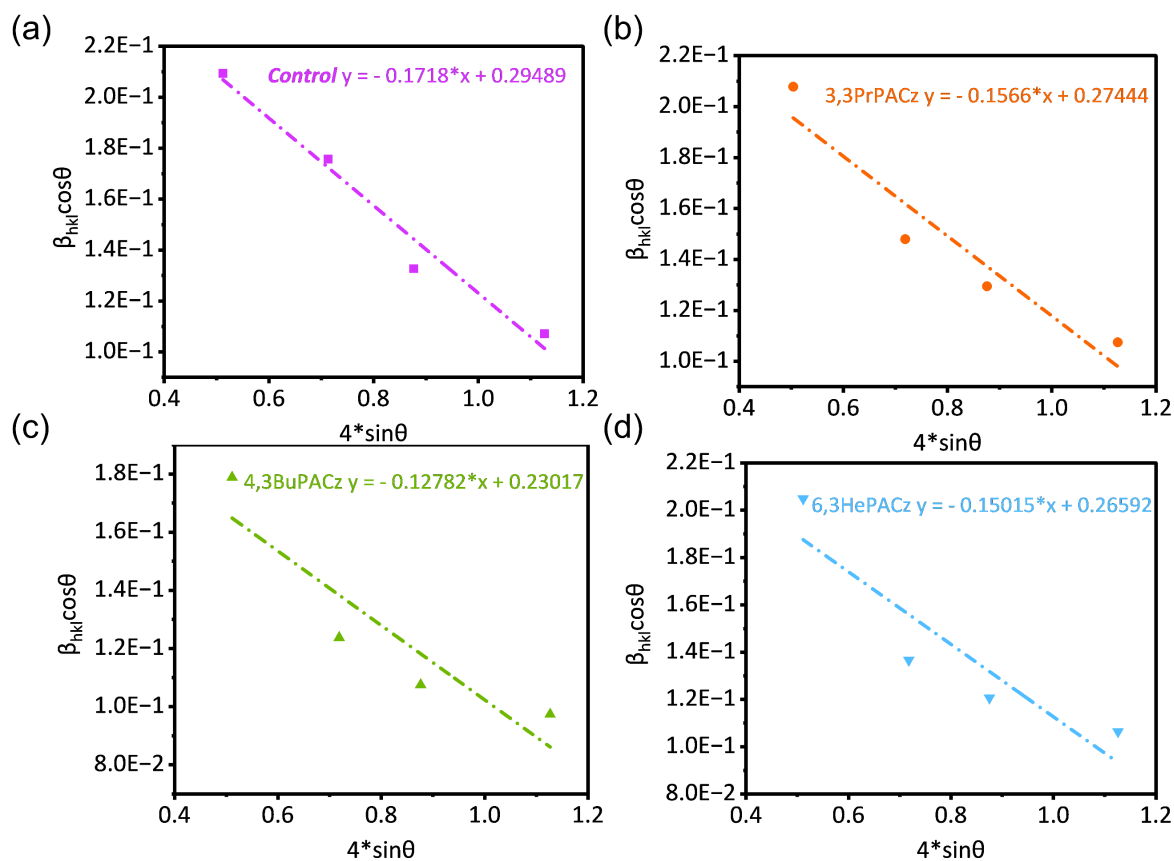


Figure S7. Williamson-Hall plot showing the variation of relative strain (slope of the fitted curve) with the perovskite film deposited on (a) PTAA, (b) PTAA/3,3PrPACz, (c) PTAA/4,3BuPACz and (d) PTAA/6,3HePACz. The effect of crystal size-induced broadening and strain-induced broadening in the half-width of XRD peaks of nanocrystals can be studied using the Williamson-Hall (W-H) method:  $\beta_{hkl}\cos\theta = 4\epsilon\sin\theta + k\lambda/d$ , where  $\beta_{hkl}$  is the angular line width at half of the maximum intensity,  $\epsilon$  is the lattice strain of the nanocrystal,  $\lambda$  is the wavelength of the X-ray radiation used and is 0.15406 nm,  $\theta$  is Bragg diffraction angle,  $k$  is the sharp factor, and  $d$  is the average crystallite size.

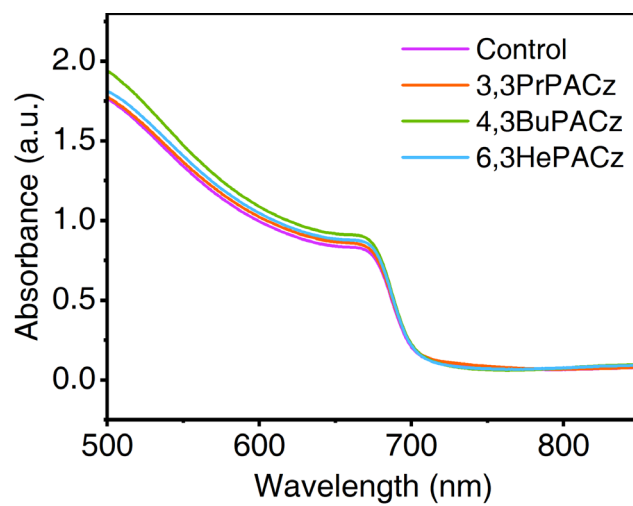


Figure S8. UV-vis absorption spectra of the perovskite films spin-coated on the different substrate.

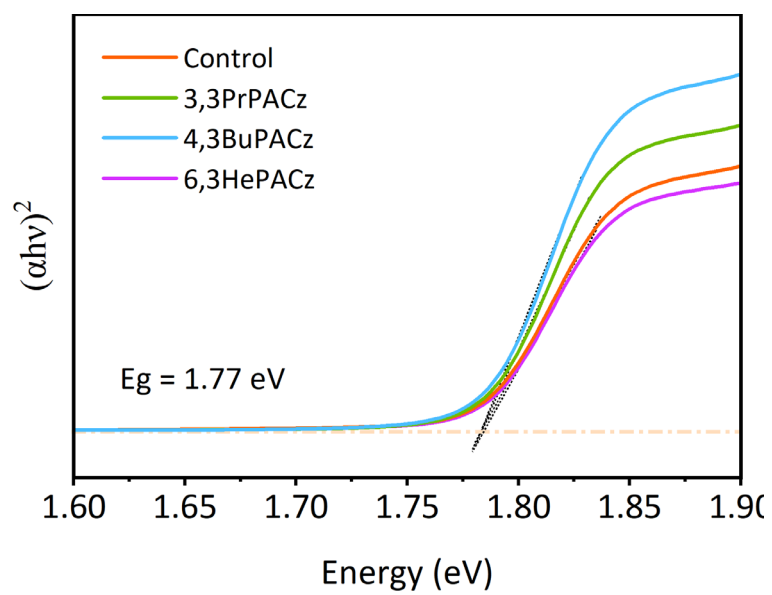


Figure S9. Bandgap of the perovskite film without or with monolayer calculate from Tauc Plot.

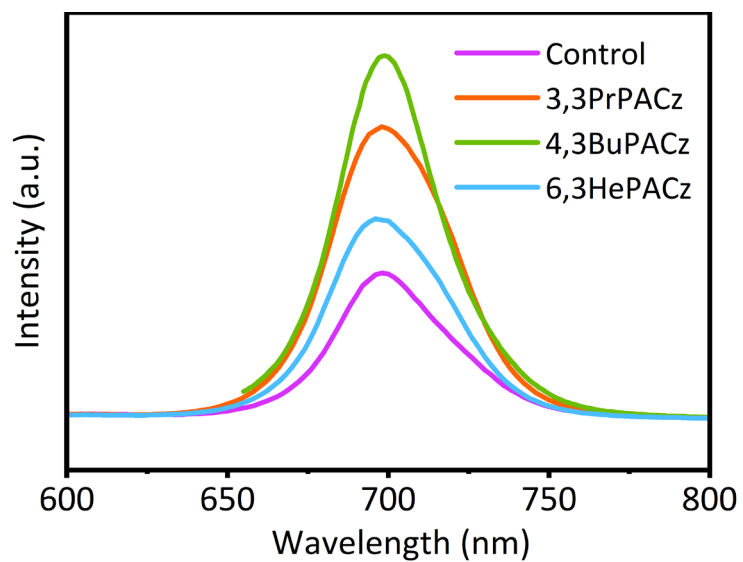


Figure S10. PL of the perovskite films deposited on non-conductive glass and monolayer-coated non-conductive glass.

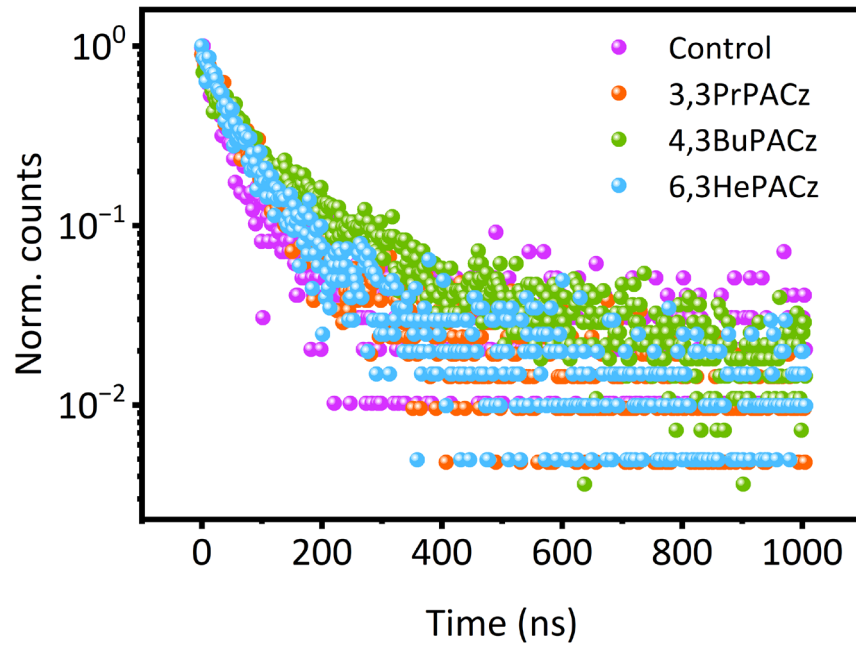


Figure S11. TRPL of the perovskite films deposited on non-conductive glass and monolayer-coated non-conductive glass.

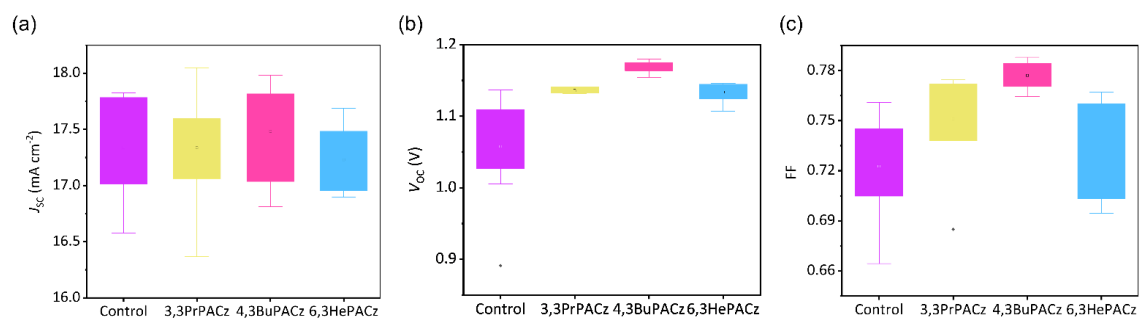


Figure S12. Statistics of (a)  $J_{sc}$ , (b)  $V_{oc}$ , and (c) FF of PSCs based on PTAA modified by different monolayer.

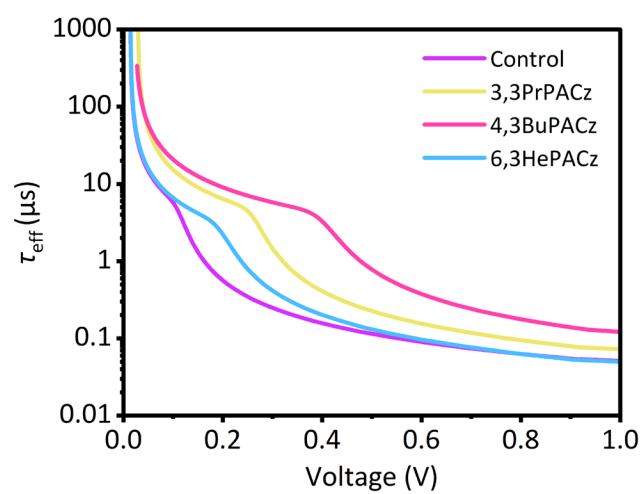


Figure S13. The effective carrier lifetimes calculated from the voltage decay curves.

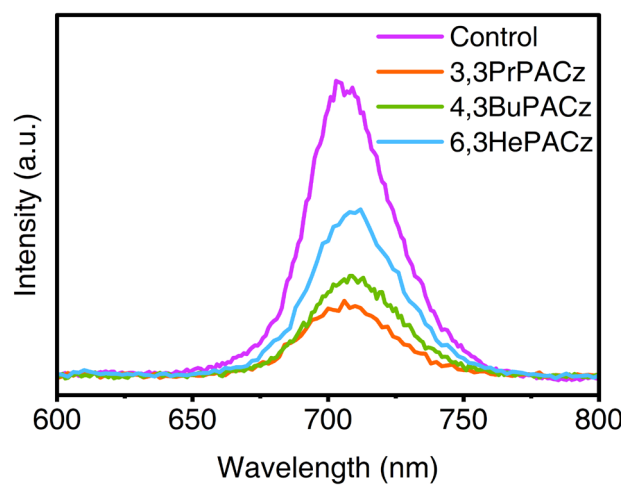


Figure S14. PL curves of the perovskite films deposited on ITO/PTAA/SAMs.

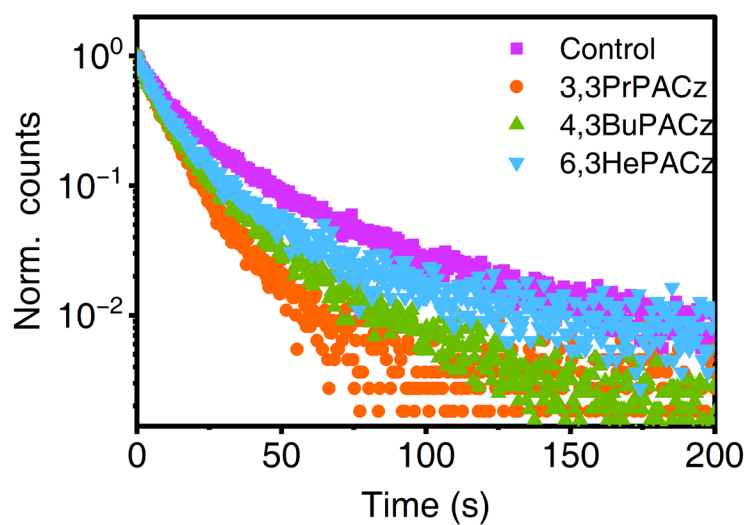


Figure S15. TRPL spectra of the control and target perovskite films with the structure of ITO/PTAA/perovskite, ITO/PTAA/3,3PrPACz/perovskite, ITO/PTAA/4,3BuPACz/perovskite, and ITO/PTAA/6,3HePACz/perovskite.

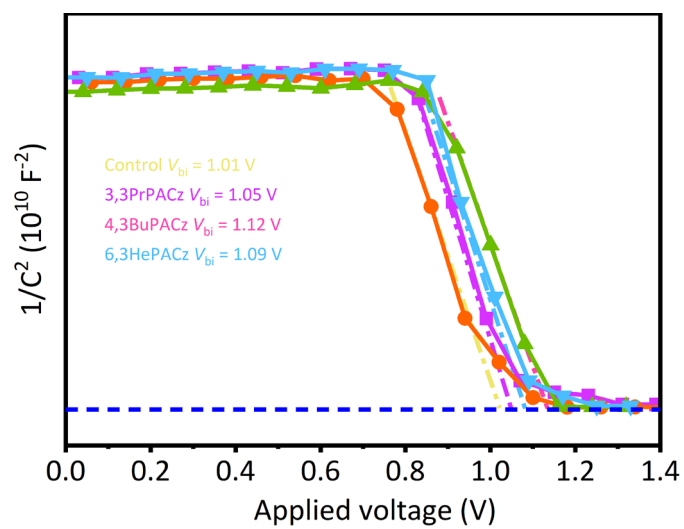


Figure S16.  $1/C^2$  as a function of the applied voltage for the control and monolayer modification devices.  $V_{bi}$  was determined by the voltage intercept of  $1/C^2$  curves.

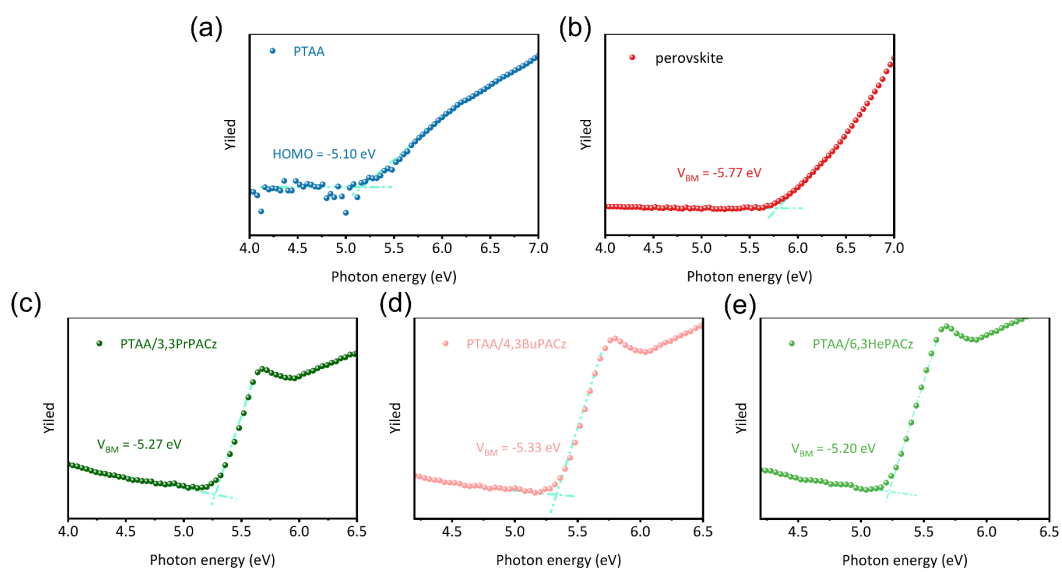


Figure S17. PYS spectra of (a) PTAA, (b) perovskite, (c) PTAA/3,3PrPACz, (d) PTAA/4,3BuPACz and (e) PTAA/6,3HePACz.

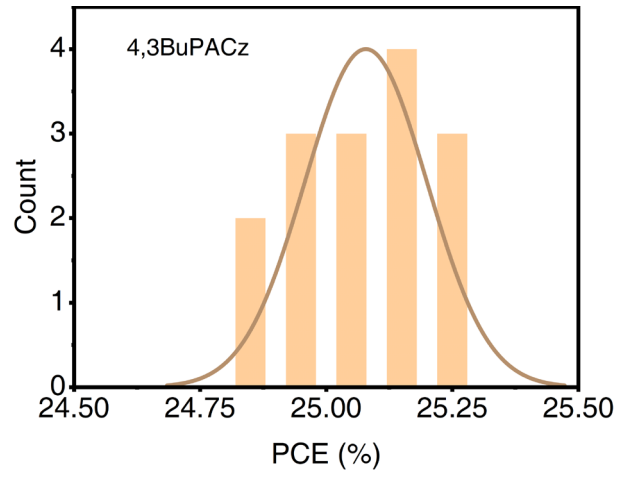


Figure S18. The statistical results of the tandem solar cells deposited on PTAA/4,3BuPACz.

Table S1 Fitted results from TRPL spectra in Figure S10.

	<b>Glass/ PVK</b>	<b>Glass/3,3PrPA Cz/PVK</b>	<b>Glass/4,3BuPA Cz/PVK</b>	<b>Glass/6,3HePA Cz/PVK</b>
$\tau_1$ (ns)	27	39	25	37
%	66	64	48	62
$\tau_2$ (ns)	88	122	139	111
%	33	36	52	38
$\tau_{ave}$ (ns)	65	92	123	85
Fitting error (1-R <sup>2</sup> ) (%)	0.32	0.27	0.30	0.29

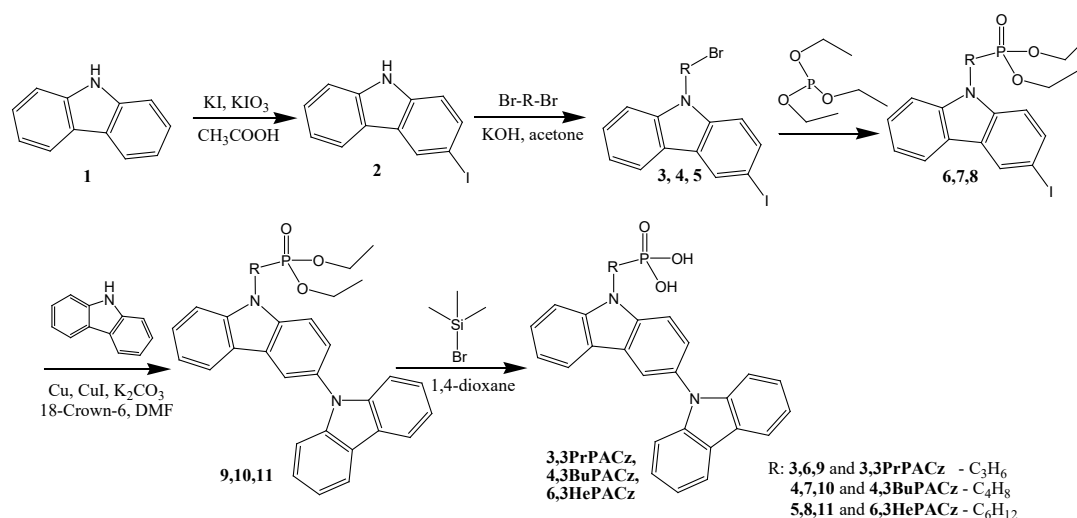
Table S2. Summary of champion and average photovoltaic parameters of the devices modified by different materials.  $J$ - $V$  curves were measured at a scan rate of 100 mV/s under simulated AM 1.5G one sun illumination of 100 mW/cm<sup>2</sup>.

		$J_{sc}$ (mA/cm <sup>2</sup> )	$V_{oc}$ (V)	FF (%)	PCE (%)
Control	<b>Champion</b>	<b>17.15</b>	<b>1.117</b>	<b>75.53</b>	<b>14.46</b>
	Average	17.33	1.057	72.26	13.28
3,3PrPACz	<b>Champion</b>	<b>17.59</b>	<b>1.141</b>	<b>77.20</b>	<b>15.49</b>
	Average	17.51	1.132	75.24	14.89
4,3BuPACz	<b>Champion</b>	<b>17.98</b>	<b>1.175</b>	<b>78.44</b>	<b>16.57</b>
	Average	17.42	1.166	77.72	15.80
6,3HePACz	<b>Champion</b>	<b>17.53</b>	<b>1.146</b>	<b>76.15</b>	<b>15.29</b>
	Average	17.23	1.133	73.59	14.38
Carbazole	<b>Champion</b>	<b>17.18</b>	<b>1.082</b>	<b>73.25</b>	<b>13.61</b>
	Average	17.12	1.085	70.42	12.4

Table S3. Fitted results from TRPL spectra in Figure S15.

	<b>ITO/PTAA/ PVK</b>	<b>ITO/PTAA/3,3 PrPACz/PVK</b>	<b>ITO/PTAA/4,3B uPACz/PVK</b>	<b>ITO/PTAA/6,3 HePACz/PVK</b>
$\tau_1$ (ns)	8	3	6	8
%	52	34	68	72
$\tau_2$ (ns)	28	13	20	27
%	48	66	32	28
$\tau_{ave}$ (ns)	23	12	14.5	19
Fitting				
error (1- R <sup>2</sup> ) (%)	0.25	0.24	0.26	0.28

Scheme S1



Scheme S1. The synthesis of bicarbazole-based SAMs was carried out by synthetic route. 3-Iodo-9H-carbazole (**2**) was obtained by procedure of Tucker as it was described earlier. Intermediate 9-bromalkylcarbazole derivatives (**3-5**) were prepared by alkylation reaction of the 3-iodo-9H-carbazole (**2**) with an excess of corresponding dibromoalkane under basic conditions of potassium hydroxide. Key starting phosphonates (**6-8**) were synthesized from commercially available triethyl phosphite and the prepared compounds **3-5**. Bicarbazole based derivatives **9-11** were then prepared by Ullmann coupling reaction of the iodo-compounds **6-8** with an excess of 9H-carbazole. The mentioned reactions were carried out in dimethylformamide (DMF) using Cu, CuI and 18-crown-6 as a catalytic system. Objective compounds as phosphonic acids: **3,3PrPACz**, **4,3BuPACz** and **6,3HePACz** were synthesized from the bicarbazole based phosphonates **9-11** by using bromotrimethylsilane in 1,4-dioxane. The newly synthesized derivatives were identified by mass spectrometry and NMR spectroscopy. The data were found to be in good agreement with the proposed structures. The derivatives were soluble in common organic solvents, such as chloroform, DMF or THF at room temperature.